



Advanced Composite Materials

Publication details, including instructions for authors and subscription information:

<http://www.tandfonline.com/loi/tacm20>

Titanium alloy foil-inserted carbon fiber/epoxy composites for cryogenic propellant tank application

Toshio Ogasawara^a, Norio Arai^b, Ryoichi Fukumoto^b, Takeshi Ogawa^b, Tomohiro Yokozeke^c & Akinori Yoshimura^a

^a Advanced Composite Research Center, Japan Aerospace Exploration Agency (JAXA), Tokyo, Japan.

^b Department of Mechanical Engineering, Aoyama-Gakuin University, Kanagawa, Japan.

^c Department of Aeronautics and Astronautics, The University of Tokyo, Tokyo, Japan.

Published online: 05 Nov 2013.

To cite this article: Toshio Ogasawara, Norio Arai, Ryoichi Fukumoto, Takeshi Ogawa, Tomohiro Yokozeke & Akinori Yoshimura (2014) Titanium alloy foil-inserted carbon fiber/epoxy composites for cryogenic propellant tank application, *Advanced Composite Materials*, 23:2, 129-149, DOI: [10.1080/09243046.2013.844756](https://doi.org/10.1080/09243046.2013.844756)

To link to this article: <http://dx.doi.org/10.1080/09243046.2013.844756>

PLEASE SCROLL DOWN FOR ARTICLE

Taylor & Francis makes every effort to ensure the accuracy of all the information (the "Content") contained in the publications on our platform. However, Taylor & Francis, our agents, and our licensors make no representations or warranties whatsoever as to the accuracy, completeness, or suitability for any purpose of the Content. Any opinions and views expressed in this publication are the opinions and views of the authors, and are not the views of or endorsed by Taylor & Francis. The accuracy of the Content should not be relied upon and should be independently verified with primary sources of information. Taylor and Francis shall not be liable for any losses, actions, claims, proceedings, demands, costs, expenses, damages, and other liabilities whatsoever or howsoever caused arising directly or indirectly in connection with, in relation to or arising out of the use of the Content.

This article may be used for research, teaching, and private study purposes. Any substantial or systematic reproduction, redistribution, reselling, loan, sub-licensing, systematic supply, or distribution in any form to anyone is expressly forbidden. Terms &

Titanium alloy foil-inserted carbon fiber/epoxy composites for cryogenic propellant tank application

Toshio Ogasawara^{a*}, Norio Arai^b, Ryoichi Fukumoto^b, Takeshi Ogawa^b,
Tomohiro Yokozeki^c and Akinori Yoshimura^a

^aAdvanced Composite Research Center, Japan Aerospace Exploration Agency (JAXA), Tokyo, Japan; ^bDepartment of Mechanical Engineering, Aoyama-Gakuin University, Kanagawa, Japan; ^cDepartment of Aeronautics and Astronautics, The University of Tokyo, Tokyo, Japan

(Received 28 May 2013; accepted 11 September 2013)

This paper presents the mechanical and gas barrier properties of titanium alloy foil-inserted carbon fiber/epoxy composites (CFRPs) undertaken to improve gas barrier properties for cryogenic propellant tank applications. A newly developed β -titanium alloy (GumMetal, GM) was applied. A sheet of titanium foil (α -Ti or GM, 0.05 or 0.1 mm) was inserted between cross-ply composite laminates ($[0^\circ_2/90^\circ_2]_S$) without adhesive. Epoxy resin in the prepreg contributes to bonding between the Ti-foil and CFRP. The Ti-alloy foil insert did not strongly affect the tensile or compressive strength. Transverse cracks in the 90° layer never penetrated into the Ti-alloy foil layer before the final failure under tensile loading. Nonlinear stress–strain behaviors attributable to the pseudo-elastic behaviors of both unidirectional CFRP and β -Ti alloy (GM) were estimated using high-order stiffness and classical lamina theory. The numerical results agreed with the experimentally obtained results. Helium gas leakage under tensile stress was not observed before the final failure of the composites (1.4% of tensile strain). The excellent mechanical and gas barrier properties were successfully demonstrated.

Keywords: carbon fiber composites; titanium alloy foil; cryogenic propellant tank; matrix crack; stress–strain behavior; gas leakage

1. Introduction

More than two decades have passed since the launch of the research and development of a cryogenic propellant tank made of carbon fiber-reinforced plastic composites (CFRP) designed to achieve weight reduction of a future space transportation system in the USA, Europe, and Japan.[1–5] However, full-fledged application of cryogenic composite tanks has not been realized not only because of the basic design management of the space transportation system, but also because of the immature technological development of the cryogenic composite tank.

An important issue related to cryogenic composite tanks is gas leakage that occurs through microscopic damage such as matrix cracks, fiber/matrix debonding, and delamination.[6–10] Matrix crack propagation occurs from low tensile strain (0.2–0.5%) at cryogenic temperatures compared with room temperature. To prevent gas leaks that

*Corresponding author. Email: ogasat@chofu.jaxa.jp

occur through the matrix microcrack network, composite overlapped pressure vessels (COPVs) have been used at room temperature. Aluminum alloy, liquid crystalline polymer, or polyamide (Nylon) is generally used for the non-structural gas-tight shell (liner). However, at cryogenic temperatures, the thermal stress attributable to the coefficient of thermal expansion (CTE) mismatch between the liner material and carbon fiber composite becomes much greater than that at room temperature.[1,11,12] Because of the severe thermal stress, debonding between a liner and CFRP occurs often. Consequently, because it is extremely difficult to design a reliable COPV for cryogenic applications, COPV usage for cryogenic propellant has not been realized anywhere in the world to date.

This study examines the use of titanium-foil-inserted carbon fiber/epoxy composites (CFRPs) to prevent gas leaks that occur through matrix microcracks. A new type of super-elastic β -titanium alloy is adopted. Titanium alloy is known to be inadequate for use in liner materials because of its incompatibility with liquid oxygen, but the titanium foil is embedded in the composite material. Therefore, the liquid oxygen never comes in contact with the Ti alloy directly. This is an additional advantage over COPV with a Ti alloy liner. The production cost of a Ti foil-inserted CFRP is much lower than that of COPV because the fabrication of a liner (thin shell) and the bonding of the liner and CFRP can be omitted.

The research and development of fiber/metal composite laminates, such as aramid fiber/aluminum, glass fiber/aluminum alloy (GLARE), and carbon fiber/titanium alloy (TiGr), have been conducted since the 1980s.[13–16] Especially, GLARE has been extremely successful: it has been used for the upper fuselage of Airbus A380. For these fiber–metal laminates, the major material is aluminum alloy or titanium alloy, and fibers are used to improve the mechanical properties of these metals. However, gas barrier properties are expected of our material. Therefore, the major material is not titanium but CFRP, and one or a few thin metal layers are sufficient to prevent gas leakage. Few research efforts on the metal foil-inserted CFRP for tank (pressure vessel) applications have been reported.[17,18] Details of stress–strain behavior, microscopic damage behavior, and gas leak behavior have not been elucidated.

A new β -Ti alloy developed in Toyota Central R&D Laboratory in 2003,[19,20] “GumMetalTM” (GM) has been examined in this study. Its chemical composition is Ti–36Nb–2Ta–3Zr–0.3O. A cold-worked GM rod specimen has low elastic modulus (40 GPa), nonlinear stress–strain behavior, high yield-strain (2.5%), and low CTE ($2 \times 10^{-6} \text{ K}^{-1}$, 77–500 K). Most of the thermomechanical properties of GM are suitable for use as a liner material of the cryogenic composite tank because the low elastic modulus and low CTE contribute to the thermal stress reduction of CFRP–metal adhesively bonded structures. However, such thermomechanical properties of GM have been reported only for cold-worked rod specimens. No experimentally obtained result has been reported for the foil or plate specimens of GM. The curious properties of GM are derived from its peculiar microstructures caused by strong cold working process. Therefore, the thermomechanical properties depend strongly on the processing.

This paper presents titanium alloy (GumMetal) foil-inserted CFRP/GM for cryogenic propellant tank application. First, the thermomechanical properties of GM foil specimens are investigated. Cross-ply CFRP/GM laminates are fabricated using a co-cure method, and the mechanical properties and microscopic damage propagation behaviors are examined in detail under tensile and compressive loading conditions. The effect of a Ti foil insert on the stress–strain behavior is calculated using classical lamina

theory (CLT). Furthermore, helium gas leak behavior of CFRP/GM specimen is evaluated at room temperature under tensile stress.

2. Experimental procedures

2.1. Mechanical properties of titanium alloy foils

GM foils were obtained from Toyota Central R&D Laboratory. A GM ingot of 250-mm diameter was made using an electron beam melting method. A plate (180-mm width, 8-mm thickness) was obtained after cold forging. Thin foils (0.05 and 0.1-mm thickness, 150-mm width) were finally obtained after several passes of cold rolling. No heat treatment was applied after the cold working. For direct comparison, α -titanium foil (0.1-mm thickness, KS40; Kobelco, Japan) was prepared.

Stress–strain behaviors of Ti and GM foils were evaluated under tensile loading at room temperature (25 °C). Tensile specimens have a width of 20 mm, and length of 60 mm. Both rolling and transverse directions were evaluated. Loading–unloading tests were also conducted for determining the yield strain. Strain was measured using a video extensometer (AVE; Instron Corp.). Tensile strength was also evaluated in liquid nitrogen (LN₂, −196 °C) and liquid helium (LHe, −269 °C), but the strain was not measured at cryogenic temperatures.

The CTE of GM was measured using GM/CFRP asymmetric laminates of 10 mm width and 140 mm length. The stacking sequence is [GM (L)/90°], [GM (T)/90°], and [GM (T)/0°]. Because of the CTE mismatch between CFRP and GM, deformation was observed as presented in Figure 1. The curvature was measured for each lamina. The CTE of GM was estimated using the following equation:

$$-(\alpha_2 - \alpha_1)\Delta T = \frac{t_1 + t_2}{2\rho} + \frac{t_1^3 E_1 + t_2^3 E_2}{6\rho(t_1 + t_2)} \left(\frac{1}{t_1 E_1} + \frac{1}{t_2 E_2} \right) \quad (1)$$

where α , E , t , and ρ , respectively, stand for CTE, Young's modulus, thickness, and curvature. Subscripts 1 and 2, respectively, denote the CFRP (0° or 90°) and GM. The CTE and elastic moduli of CFRP are, respectively, $-0.5 \times 10^{-6} \text{ K}^{-1}$ and 153 GPa for the 0 direction, and $22 \times 10^{-6} \text{ K}^{-1}$ and 8.2 GPa for the 90° direction.[6]

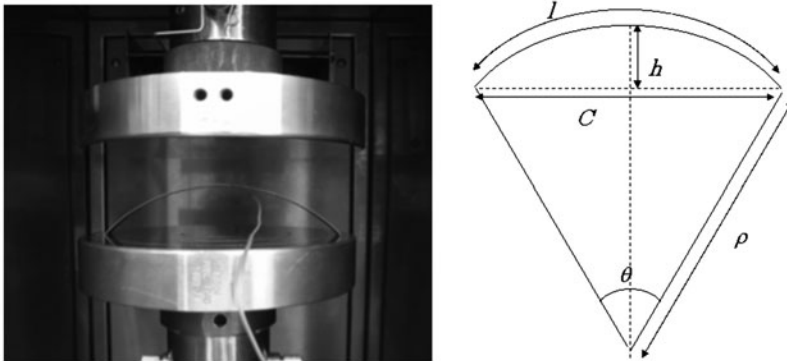


Figure 1. Evaluation of the CTE of β -titanium alloy (GM) using CFRP/GM asymmetric laminate.

2.2. Composite materials and specimens

Unidirectional carbon fiber/toughened epoxy prepreg tape (IM600/QC133) was obtained from Toho Tenax Co. Ltd. (Japan). Prepreg sheets were cut into 220 x 220 mm pieces, and a piece of titanium foil (220 x 220 mm) was embedded in the middle of a cross-ply laminate as presented in Figure 2(a). The rolling direction of Ti foil is parallel to the specimen's longitudinal direction. CFRP/Ti and CFRP/GM were fabricated using a co-curing process. No adhesive was used for bonding Ti foil to CFRP. Therefore, only the epoxy resin in the prepreg contributes to the bonding of the Ti foil and CFRP. The stacking sequence is $[0_2/90_2]_S$ for CFRP and $[0_2/90_2/(Ti \text{ or } GM)/90_2/0_2]$ for CFRP/Ti, or CFRP/GM. The thickness of each layer is double of the prepreg thickness to make the observations of microscopic damage (transverse cracks) easy. The fiber volume fraction (Vf) was 55%. The nominal prepreg thickness was 0.135 mm. The titanium foil surface was ground using emery paper (#600) and was washed with acetone using a supersonic cleaner. A Ti foil was sandwiched between the carbon fiber prepreg sheets and was cured at 180 °C for 2 h under 0.5 MPa in a hot press.

Model specimens for simulating seam joints of Ti foils were also prepared because the joining of Ti foil is indispensable for future construction of a large composite tank structure. Figure 2(b)–2(d), respectively, show a butt splice, lap splice without adhesive, and lap splice with adhesive. The lap lengths were 2 and 5 mm for Figure 2(c), and 2 mm for Figure 2(d). Epoxy film adhesive (AF163; 3M Co., USA) was used for the lap splice presented in Figure 2(d).

2.3. Evaluation of the mechanical properties of the composite materials

Apparent interlaminar shear strengths were measured using a short-beam bending (SBS) method in accordance with JIS-K7078 under a constant displacement rate of 1 mm/min on a mechanical test rig (5580; Instron Corp., USA). The five SBS specimens had 2 mm thickness, 10 mm width, and 20 mm length. Lower span width was 11.2 mm. The respective upper roller and lower roller radii were 5 and 2 mm.

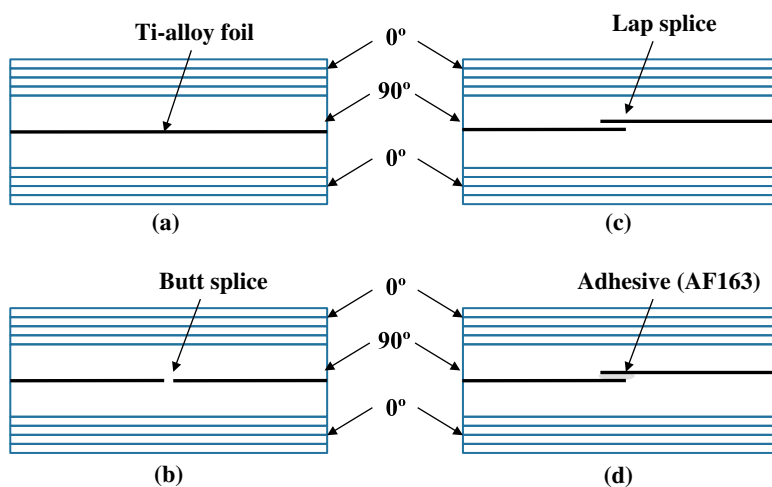


Figure 2. Schematic drawing of Ti-foil inserted CFRPs: (a) seamless, (b) butt splice, (c) lap splice without adhesive, and (d) lapsplce with adhesive.

Tensile tests were conducted at room temperature (25 °C) and cryogenic temperature (−196 °C) under a constant displacement rate of 0.5 mm/min on a mechanical test rig (8802; Instron Corp., UK). Strip-type specimens of 10 mm width, 100 mm gage length, 50 mm grip length, and 200 mm overall length were used for the tensile tests. Longitudinal and transverse strains were measured using electrical resistance strain gages. Acetyl cellulose film was used to obtain a replica of the specimen surfaces for microscopic damage observations under tensile loading. Four CFRP specimens and five CFRP/Ti and CFRP/GM specimens were used.

Compressive tests were conducted at room temperature on a mechanical test rig (5582; Instron Corp., UK) under a constant displacement rate of 0.5 mm/min in accordance with NAL-II method [21] as proposed by the authors. Specimens have 15 mm width, 16 mm gauge length, 80 mm overall length, and 2.2 thickness. The number of specimens were five each.

2.4. Evaluation of helium gas leak behavior

The stacking sequences of specimens used for helium gas leak testing were $[0_2/90_2]_S$ and $[0_2/90_2/GM(L)/90_2/0_2]_S$. Gas leak behavior of CFRP/Ti composite was not evaluated, because the mechanical properties and transverse crack growth behaviors are almost the same as that of CFRP/GM composite. Specimens have 40 mm width, 100 mm gauge length, 50 mm grip length, and 200 mm overall length. Details of the test procedure have been reported elsewhere.[7] Before gas leak testing, three-point bending load was applied to induce matrix cracking of the surface 0 layers as shown in Figure 3. The lower span length was 30 mm. The bending test was interrupted immediately after a slight load drop with audible sound. This operation was conducted for another surface.

Helium gas leak was measured using a helium leak detector (MSE-3000; Shimadzu Corp., Japan). Stainless steel jigs were set on both sides of a tensile specimen as portrayed in Figure 4. The test area was 45×25 mm. Helium gas flowed on the one side surface of a sample at 50 ml/min. The opposite surface was evacuated using the vacuum pump of the leak detector. Therefore, the pressure difference was 0.1 MPa. The helium leak rate, J ($\text{Pa m}^3/\text{s}$), was measured at room temperature (25 °C).

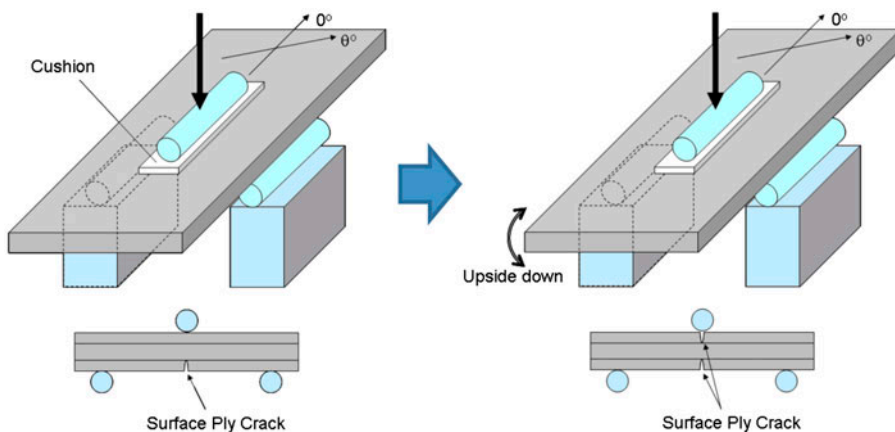


Figure 3. Three-point bending test for surface ply crack induction.

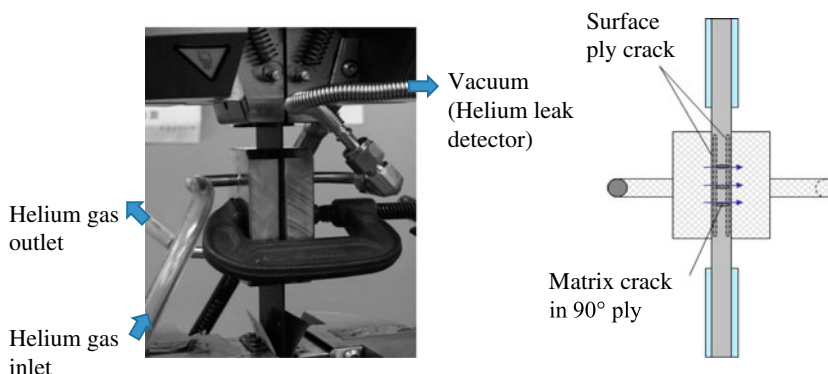


Figure 4. Helium gas leak measurement under uniaxial tension load.

When transverse cracks in the 90° layer propagate under tensile loading, gas leak paths are formed by a combination of the transverse cracks in the 90° layer and the matrix crack in the 0° layer derived from the preliminary three-point bending load.

3. Results and discussion

3.1. Thermomechanical properties of GM foils

Stress–strain curves of α -Ti and GM foils under monotonic tensile loading are presented as open circles in Figure 5. Therein, T and L, respectively, denote longitudinal and transverse direction of the cold rolling process. The Young's modulus (E), ultimate tensile strength (UTS) (σ_B), failure strain (ϵ_B), 0.2% yield stress ($\sigma_{0.2}$), and yield strain (ϵ_Y) are presented in Table 1. α -Ti (KS40) has typical elastic/plastic behavior. The yield stress and strain were approximately 190–220 MPa and 0.47–0.5%. The stress hardening factor (n) was 0.23. Data of typical β -Ti alloy (Ti-13 V-11Cr-3Al) and α/β -Ti alloy (Ti-6Al-4 V) available from the literature are shown in Table 1 for direct comparison.

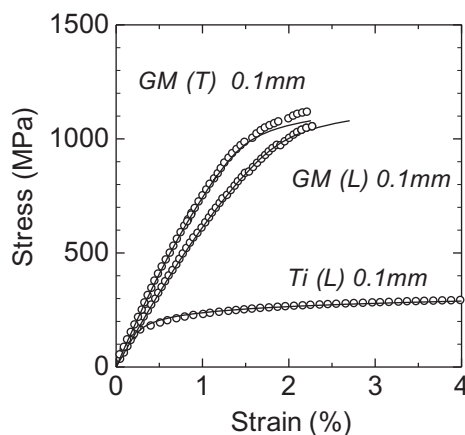


Figure 5. Stress–strain curves of titanium alloy foils obtained from tensile testing at room temperature. Symbols denote the experimentally obtained results. Solid lines show numerical results based on nonlinear elastic model and Hill's plasticity model.

Table 1. Mechanical properties of α -Ti, GM, β -Ti alloy and α - β Ti alloy.

| | α -Ti (JIS 1 grade) KS40 | | GumMetal (GM) (Ti-36Nb-2Ta-3Zr- 0.3O) | | β -Ti alloy* | α/β -Ti alloy** |
|-------------------------------------|---------------------------------------|-------|---|---------|--------------------|----------------------------|
| Direction | L | T | L | T | — | — |
| Elastic modulus, E_x (GPa) | 74.7 | 109.9 | 72.0 | 80.0 | 100 | 114 |
| Tensile strength, σ_B (MPa) | 316.0 | 302.9 | 1068 | 1114 | 1280 | 1170 |
| Tensile strain, ε_B (%) | 12.0 | 9.7 | 2.6 | 2.2 | — | — |
| Yield stress, $\sigma_{0.2}$ (MPa) | 187 | 225 | 741-863 | 860-989 | 1210 | 1100 |
| Yield strain, ε_Y (%) | 0.471 | 0.498 | 1.2-1.5 | 1.2-1.5 | — | — |
| CTE (K^{-1}) $\times 10^{-6}$ | 8.4 | — | 6.18 | 5.40 | 8.5 | 8.6 |

*Ti-13V-11Cr-3Al, STA, **Ti-6Al-4V, STA (Data from “Structure and Properties of Engineering Alloys Second Edition”, W. F. Smith, McGraw-Hill Inc. NY 1990.)

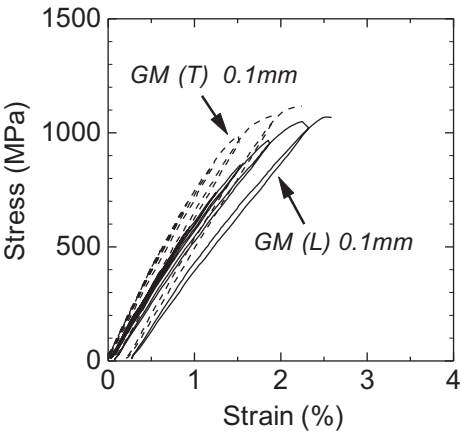


Figure 6. Stress-strain curves of β -titanium alloy (GM) obtained by loading-unloading tensile testing.

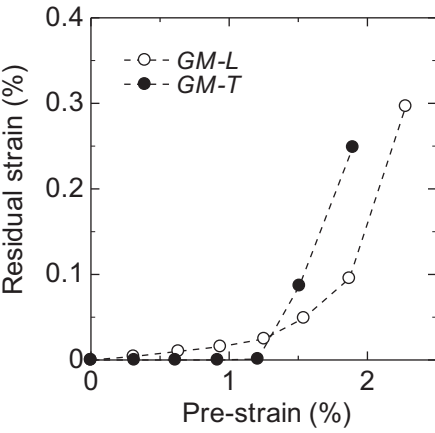


Figure 7. Residual strain vs. pre-strain of β -titanium alloy (GM).

Stress–strain curves of GM obtained from loading–unloading tests are depicted in Figure 6, and the relation between the maximum strain and residual strain are presented in Figure 7. GM foil exhibits considerable nonlinear stress–strain behaviors above 0.3% strain. The nonlinear behavior is pseudo-elastic below 1.5% strain (850 MPa tensile stress) because no residual strain at zero stress after the unloading step was observed in Figures 6 and 7. Both α -Ti and GM show slightly anisotropic behavior for longitudinal and transverse rolling directions.

High-order elastic stiffness is adopted for GM as follows.[22]

$$\varepsilon_1 = (S_{11} + S_{111}\sigma_1 + S_{1111}\sigma_1^2)\sigma_1 \quad (2)$$

Estimates of elastic moduli (high order stiffness) are presented in Table 2.

Hill's plasticity theory for modeling plastic flow in anisotropic materials is applied for evaluating the stress–strain curves of Ti and GM. Assuming the plain stress condition, the effective stress and effective strain are expressed as the following equations [23,24]:

$$\bar{\sigma} = h(\theta)\sigma_x \quad (3)$$

$$\bar{\varepsilon}^p = \varepsilon_x^p/h(\theta) \quad (4)$$

with

$$h(\theta) = \left[\frac{3}{2} (\cos^4 \theta + a_{22} \sin^4 \theta + 2 \cos^2 \theta \sin^2 \theta) \right]^{1/2}, \quad (5)$$

where σ_x and ε_x^p are related respectively to the uniaxial loading stress and the plastic strain. Subscripts 1 and 2 denote longitudinal (L) and transverse (T) directions along the cold rolling process. The coefficients a_{22} describe the degree of anisotropy in the plasticity as determined from experimental data. A power law is used to fit the master effective stress – effective plastic strain curve:

$$\bar{\sigma} = A \cdot \ln(\bar{\varepsilon}^p) + B \quad (6)$$

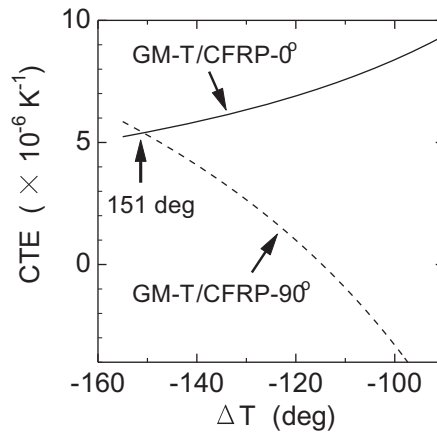
The estimated parameters a_{22} , A , and B of Ti and GM are presented in Table 3. Numerical results obtained using these parameters are superimposed on Figure 5 as solid lines. The numerical results show good agreement with the experimentally obtained data. The coefficient a_{22} is 0.97 for α -Ti and 0.93 for GM, which implies that the plastic deformation behavior is almost isotropic in spite of anisotropic pseudo-elastic behavior.

Table 2. High-order stiffness of GM and IM600/133.

| | S_{11} (1/MPa) | S_{111} (1/MPa ²) | S_{1111} (1/MPa ³) |
|---------------------|-----------------------|---------------------------------|----------------------------------|
| GM (L direction) | 1.51×10^{-5} | -4.27×10^{-10} | 4.08×10^{-12} |
| GM (T direction) | 1.15×10^{-5} | 7.60×10^{-10} | 2.48×10^{-12} |
| UD-CFRP (IM600/133) | 6.95×10^{-6} | -5.88×10^{-10} | 1.35×10^{-13} |

Table 3. Orthotropic plastic parameters of α -Ti and GM in Hill's plasticity model.

| | a_{22} | A (MPa) | B (MPa) |
|--------------|----------|-----------|-----------|
| α -Ti | 0.97 | 37.4 | 188.5 |
| GM | 0.93 | 58.1 | 362.6 |

Figure 8. CTE as a function of ΔT evaluated using Ti alloy/CFRP asymmetric beam method.

The CTE of the GM rolling direction (L) calculated from the curvature of [GM(T)/90°] and [GM(T)/0°] asymmetric laminates is presented in Figure 8 as a function of temperature difference ΔT . Therein, ΔT is defined as the difference between the stress-free temperature and room temperature. The CTE estimated from [GM(T)/90°] laminate is identical to that estimated from [GM(T)/0°] laminate at $\Delta T = 151^\circ$. The curing temperature was 180°C ($\Delta T = 180 - 25^\circ\text{C} = 155^\circ$). Therefore, this value (151°) is quite reasonable. As result, the CTE of GM L-direction is estimated as $6.2 \times 10^{-6} \text{K}^{-1}$, which is lower than that of other titanium alloys, as shown in Table 1. However, the CTE of GM foil is much higher than that of a cold-forged rod specimen ($1-2 \times 10^{-6} \text{K}^{-1}$). [16]

Reportedly, cold-forged rod specimens of GM exhibit lower elastic modulus, higher yield strain, and lower CTE than those of general β -titanium alloys. However, lower CTE and lower Young's modulus were not observed in foil specimens. It has been reported that the curious thermomechanical properties of GM derive from residual stress and microstructures caused by strong cold-forging process. [25,26] In the case of foil, the residual stress caused by the foil forming process is not high compared to that

Table 4. UTSs of GM at room and cryogenic temperatures.

| Temperature | Ultimate tensile strength (MPa) | |
|---------------------------|---------------------------------|-------------------|
| | L direction | T direction |
| RT (25 °C) | 1068 (1070, 1066) | 1114 (1118, 1110) |
| LN ₂ (−196 °C) | 1844 (1862, 1826) | 1791 (1819, 1763) |
| LHe (−269 °C) | 1988 (2016, 1959) | 2018 (2034, 2002) |

Notes: Values in brackets denote raw data.

Number of specimen is two.

obtained from rod-forging processes. However, GM has low elastic modulus, high strength, and low CTE for direct comparison with the literature data of α/β -Ti alloy (Ti-6Al-4 V) and β -Ti alloy (Ti-13 V-11Cr-3Al) as shown in Table 1. GM is inferred to be suitable for use in combination with CFRP.

UTSs in liquid nitrogen and liquid helium are presented in Table 4. The tensile strength increases continuously with decreasing test temperatures. The tensile strength in LHe (-269°C) is approximately 2 GPa, which is about double that that at room temperature.

3.2. Tensile behavior of cross-plyed CFRP, CFRP/GM, and CFRP/Ti

Stress–strain curves of CFRP, CFRP/GM, and CFRP/Ti are presented in Figures 9–11 as open circles. The tensile strength and Young's modulus are shown respectively in Tables 5 and 6. Nonlinear stress–strain behavior was observed in stress–strain curves. Therefore, the Young's modulus was calculated as 0.1–0.3%, and as 0.1–1.0% of strain using linear regression. A slight decrease in the Young's modulus is observed when inserting Ti and GM foil in CFRP. The tensile strength of CFRP/GM is almost identical to that of CFRP, whereas the strength of CFRP/Ti slightly decreases. An optical micrograph illustrating the side surface of CFRP/GM specimen subjected to 1.2% of tensile strain is presented in Figure 12(a) and 12(b). Transverse cracks propagated in the 90° layer are readily apparent; the cracks arrest at the interface between the 90° layer and GM foil. No delamination was observed at the interface at 0.7%, and a little delamination was visible at 1.2%. The bonding strength between CFRP and GM is sufficient to arrest the transverse cracks in the 90° layer.

Reportedly, unidirectional carbon fiber composites (0°) exhibit nonlinear stress–strain behavior,[22,27,28] which is caused by the microstructure of carbon fiber itself. [29] The stress–strain curves of unidirectional CFRP used for this study are presented in Figure 13, which was obtained from tensile and compressive testing. Nonlinear stress–strain behavior is observed continuously from compression to tension loading conditions. The nonlinear behavior is not plastic deformation but pseudo-elastic deformation in this strain range because no residual strain was observed in loading–unloading tests. The estimated high-order stiffness parameters are presented in Table 2.

Table 5. Average values of tensile and compressive strengths of CFRP, CFRP/GM, and CFRP/Ti.

| | Temp. | Number of plies | CFRP | CFRP/GM 0.05 mm | CFRP/GM 0.1 mm | CFRP/Ti 0.1 mm |
|------------------------------------|-------|-----------------|-----------------|--------------------|-------------------|-------------------|
| Tensile Strength (MPa) | RT | 16 ply | 1396 (50.6) | 1406 (24.2) | 1390 (34.3) | 1413 (21.2) |
| | | 8 ply | 1390 (32.5) | 1385 (22.9) | 1408 (64.5) | 1299 (63.8) |
| | LN2 | 8 ply | 1266 (86.0) | 1270 (16.3) | 1287 (46.6) | 1205 (30.6) |
| | | 16 ply | 559.1 (19.9) | 562.3 (19.1) | 559.8 (24.4) | 547.6 (40.1) |
| Compressive strength (MPa) | RT | 16 ply | 89.2 (1.4) | 91.4 (3.0) | 95.0 (2.2) | 92.4 (2.3) |
| Short beam shear strength (MPa) | RT | 16 ply | | | | |

Note: Values in brackets denote standard deviations.

Table 6. Average values of Young's modulus of CFRP, CFRP/GM, and CFRP/Ti under tensile and compressive loading conditions.

| | Temp. | Strain range (%) | CFRP | CFRP/GM 0.05 mm | CFRP/GM 0.1 mm | CFRP/Ti 0.1 mm |
|---------------------------|-------|------------------|------|--------------------|-------------------|-------------------|
| Tensile modulus (GPa) | RT | 0.1–0.3 | 82.0 | 79.5 | 78.6 | 78.1 |
| | | 0.1–1 | 86.7 | 84.2 | 83.1 | 82.0 |
| Compressive modulus (GPa) | RT | 0.1–0.3 | 74.7 | 74.2 | 77.2 | 77.6 |
| | | 0.1–0.6 | 71.5 | 72.6 | 73.0 | 74.4 |

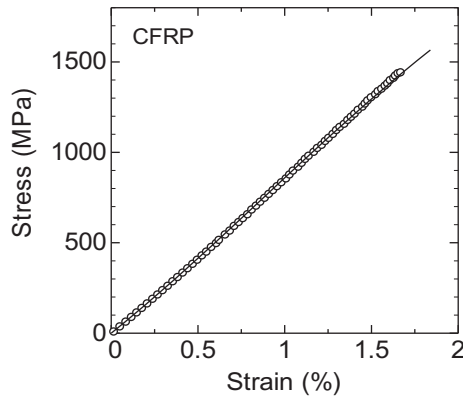


Figure 9. Stress–strain curve of cross-ply carbon/epoxy laminate (CFRP) obtained by tensile testing. Open circles and the solid curve respectively denote the experimental and predicted results.

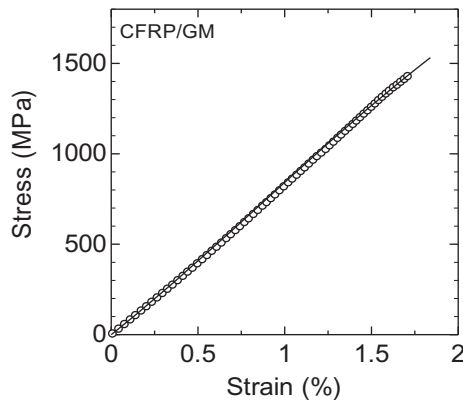


Figure 10. Stress–strain curve of GM foil-inserted carbon/epoxy laminate (CFRP/GM) obtained by tensile testing. Open circles and the solid curve respectively denote the experimental and predicted results.

Both GM and CFRP exhibit pseudo-elastic behavior. Therefore, the stress–strain curve of CFRP/GM is estimated using nonlinear elastic constituent equation (Equation (2)) and CLT. The initial elastic modulus of CFRP/GM differs slightly from that of CFRP presented in Figure 13. Therefore a correction factor (0.96) was multiplied by the stiffness parameters (S_{11} , S_{111} , S_{111}) in Table 2. This is probably attributable to the

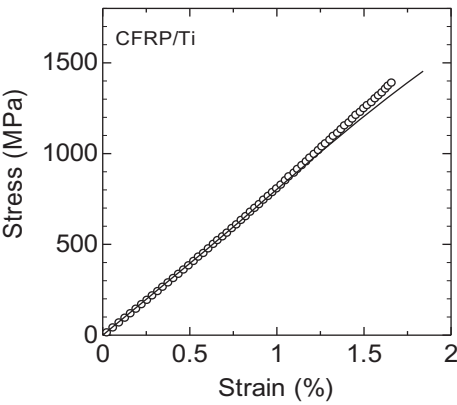


Figure 11. Stress–strain curve of Ti foil-inserted carbon/epoxy laminate (CFRP/Ti) obtained by tensile testing. Open circles and solid curve respectively denote the experimental and predicted results.

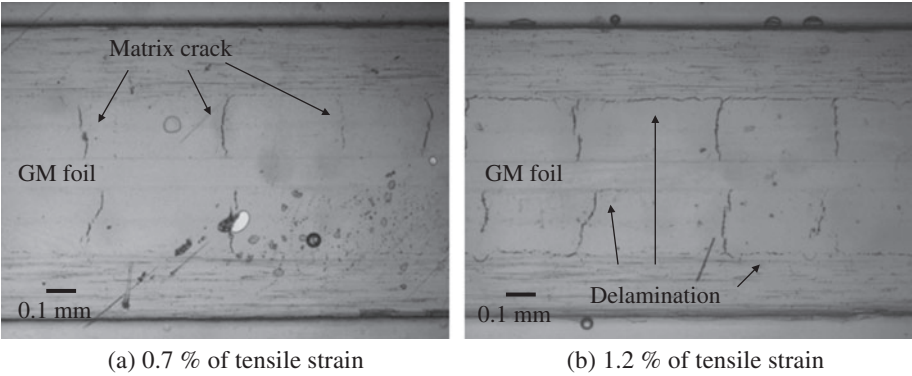


Figure 12. Optical micrographs of acetyl cellulose replica films showing the CFRP/GM side surface.

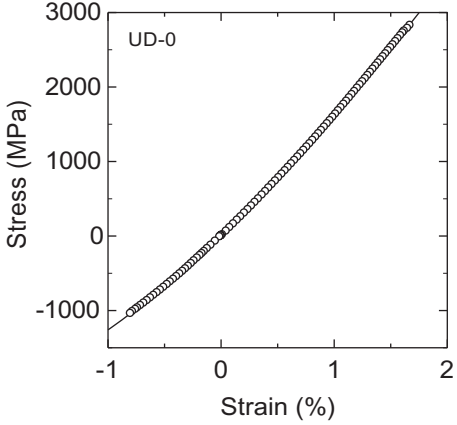


Figure 13. Stress–strain curve of unidirectional CFRP obtained by tensile and compressive tests. Open circles and solid curve respectively show the experimental and predicted result.

Table 7. Estimated Young's modulus of CFRP, CFRP/GM, and CFRP/Ti using high-order stiffness (Table 2) and CLT.

| | Temp. | Strain range (%) | CFRP | CFRP/GM 0.05 mm | CFRP/GM 0.1 mm | CFRP/Ti 0.1 mm |
|---------------------------|-------|------------------|------|--------------------|-------------------|-------------------|
| Tensile modulus (GPa) | RT | 0.1–0.3 | 82.1 | 81.4 | 80.8 | 79.3 |
| | | 0.1–1 | 86.9 | 86.0 | 85.1 | 80.3 |
| Compressive modulus (GPa) | RT | 0.1–0.3 | 74.4 | 74.2 | 74.1 | 74.7 |
| | | 0.1–0.6 | 71.6 | 71.4 | 71.3 | 71.3 |

difference in the fiber V_f of CFRP. An elastic–plastic constituent model was assumed for α -Ti. The initial elastic modulus is 80 MPa, and yield stress is 200 MPa. The plastic constraint was ignored for the calculation. The effect of thermal stress was examined assuming the temperature difference ΔT of 150°.

Numerical results are presented in Figures 9–11 as solid curves. The estimated Young's moduli are shown in Table 7. The numerical results of CFRP and CFRP/GM show good agreement with the experimental data up to the final failure, which implies that nonlinear elastic model and CLT are effective to estimate the stress–strain behavior of CFRP/GM. However, discrepancies between the numerical and experimentally obtained results are observed in CFRP/Ti. Because the plastic constraint was ignored for the calculation, the CFRP/Ti stiffness was underestimated.

3.3. Matrix crack propagation in cross-plyed CFRP, CFRP/GM, and CFRP/Ti

The relation between transverse crack density and tensile strain of CFRP, CFRP/GM, and CFRP/Ti is presented in Figure 14. The crack density is the number of transverse cracks per unit length (1 cm). In the case of CFRP/GM and CFRP/Ti, the number of transverse cracks was defined as half of the total number of transverse cracks observed in two 90° layers.

Transverse cracks arrested at the interface between the titanium foil and CFRP and the damage in the titanium foil are not observed up to 1.3% of tensile strain. The onset

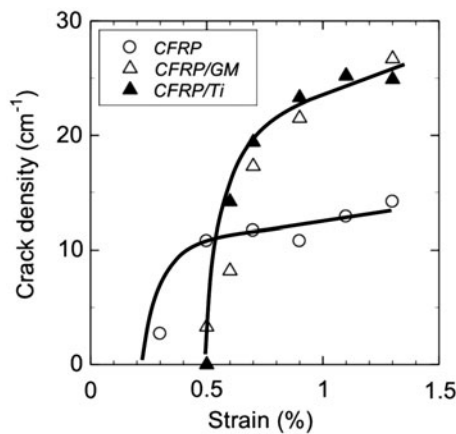


Figure 14. Transverse crack density vs. strain of CFRP, CFRP/GM and CFRP/Ti cross ply laminates.

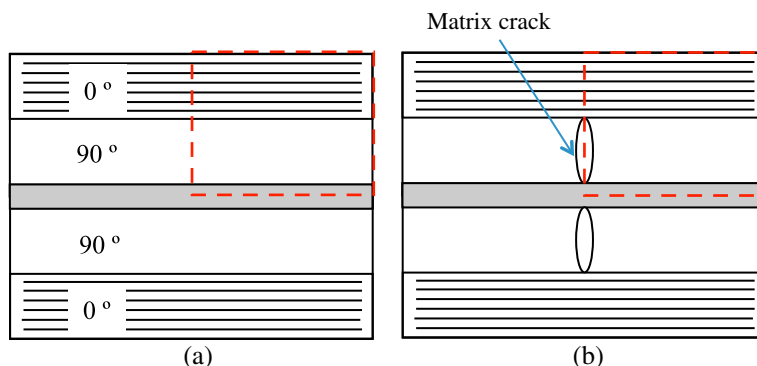


Figure 15. Finite element analysis model for calculating strain energy release rate caused by transverse crack propagation in the 90 layer. The strain energy balance between (a) and (b) is calculated.

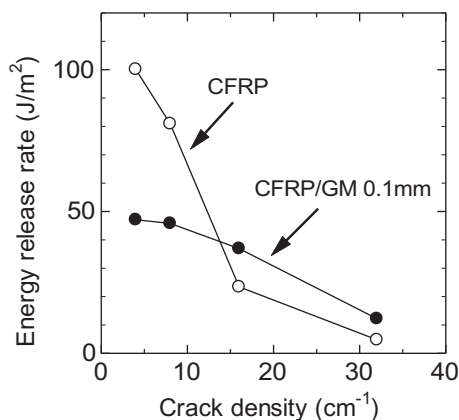


Figure 16. Strain energy release rate of CFRP and CFRP/GM cross-ply laminates as a function of crack density.

of transverse crack propagation is about 0.3% for CFRP, and 0.5% for CFRP/GM and CFRP/Ti. Transverse crack densities in CFRP/Ti and CFRP/GM are greater than that in CFRP above 0.7% of tensile strain.

The strain energy release rate caused by the transverse crack propagation was calculated using finite elementary analysis (FEA) with the FEA model presented in Figure 15(a) and (b). The strain energy release rate was determined by substituting the strain energy without a crack and with a crack. A commercial FEA code, ABAQUS, was used for the calculation. The numerical results are presented in Figure 16 as a function of the crack density. The strain energy release rate of CFRP is higher than that of CFRP/GM below 10 cm⁻¹ of crack density. This result agrees qualitatively with the experimentally obtained results.

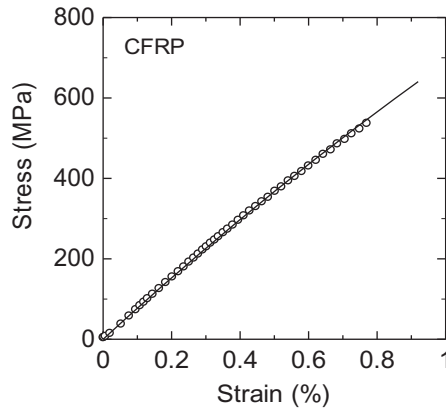


Figure 17. Stress-strain curve of carbon/epoxy laminate (CFRP) obtained by compressive testing. Open circles and the solid curve respectively show the experimental and predicted result.

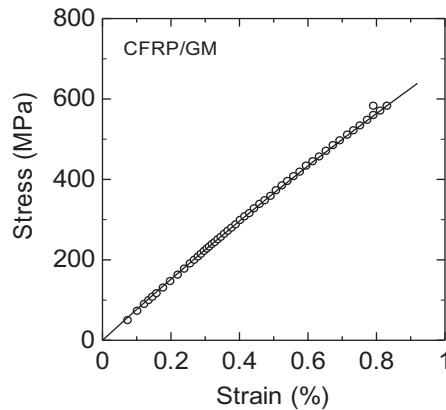


Figure 18. Stress-strain curve of carbon/epoxy laminate (CFRP/GM) obtained by compressive testing. Open circles and solid curve respectively show the experimental and predicted result.

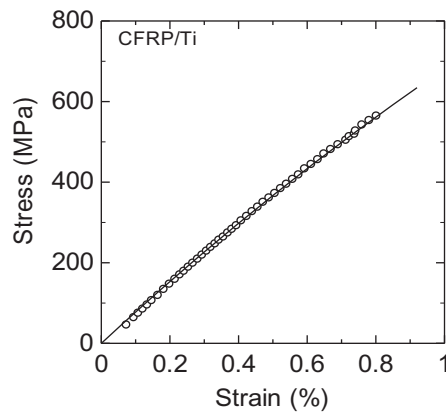


Figure 19. Stress-strain curve of carbon/epoxy laminate (CFRP/Ti) obtained by compressive testing. Open circles and solid curve respectively show the experimental and predicted result.

Table 8. Compressive strengths of lap-splice CFRP/GM without adhesive.

| Lap length (mm) | CFRP/GM 0.05 mm | CFRP/GM 0.1 mm |
|-----------------|-----------------|----------------|
| 2 | 558 | 570 |
| 5 | 570 | 577 |

3.4. Compressive behaviors of cross-plyed CFRP, CFRP/GM, and CFRP/Ti

Stress–strain curves of CFRP, CFRP/GM, and CFRP/Ti are presented as open circles in Figures 17–19. The average compressive strengths and Young's moduli are presented in Tables 5 and 6. Nonlinear stress–strain behavior is also shown there. The Young's moduli were calculated as 0.1–0.3% and 0.1–0.6% using linear regression. Both the strength and elastic modulus are unaffected by insertion of Ti or GM foil in cross-plyed CFRP.

Stress–strain curves of CFRP/Ti and CFRP/GM were calculated using the nonlinear elastic model (Equation (2)) and CLT. In this case, a correction factor (0.98) was multiplied by the elastic parameters (S_{11} , S_{111} , S_{1111}) in Table 2 so that the initial elastic modulus of CFRP is identical to the numerical result. Numerical results are presented in Figures 17–19 as solid curves, and in Table 7. The numerical results show good agreement with the experimentally obtained results up to the point of final failure. Although the effect of microscopic damage is not considered for the calculation, this method is effective to estimate the stress–strain behavior of CFRP/GM and CFRP/Ti under both tensile and compressive stress.

The respective compressive strengths of butt splice and lap splice specimens are presented in Table 8. Splice and lap lengths do not affect the compressive strength well. Titanium foil was embedded in the 90° layer. Therefore, the lap splice does not affect the fiber misalignment of the 0° layer to any considerable degree, resulting in no degradation in compressive strength.

The tensile and compressive properties of CFRP/GM are almost same as those of CFRP/Ti composites. The advantage of GM has not been clearly demonstrated as compared with pure Ti. It is concluded that the tensile strength, stress–strain behavior,

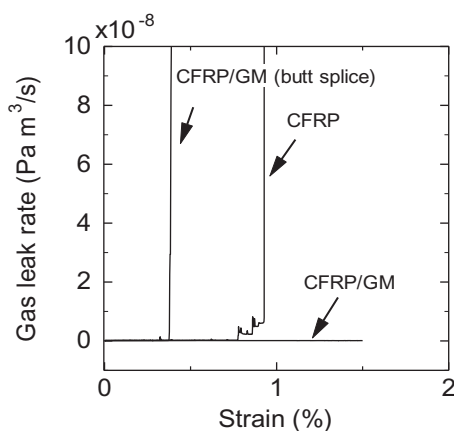


Figure 20. Helium gas leakage rates of CFRP, CFRP/GM (seamless), and CFRP/GM (butt splice joint) cross-ply laminates as a function of tensile strain.

and transverse crack growth behavior of both CFRP/GM and CFRP/Ti are suitable for cryogenic propellant tank applications.

3.5. Helium gas leak behavior of CFRP and CFRP/GM

The helium gas leakage rates of CFRP and CFRP/GM under tensile loading are presented in Figure 20 as a function of tensile strain. Considerable gas leakage was observed clearly around 0.8% of strain for CFRP. The maximum leak rate was $2.1 \times 10^{-5} \text{ Pa m}^3/\text{s}$. X-ray radiography of a CFRP specimen showing that it is not subjected to tensile load is presented in Figure 21(a). A matrix crack propagating parallel to the specimen longitudinal direction was induced during the initial bending load, as depicted in Figure 3. After tensile loading, many transverse cracks were observed, as presented in Figure 21(b). Intersection points between matrix cracks in the 0° layer and those in the 90° layer become leakage paths of helium gas. No gas leakage was observed for CFRP/GM up to 1.4%, which is the point of failure strain. Titanium foil acts as an excellent gas-tight layer. However, the gas leak occurred only at 0.4% for the butt-spliced CFRP/GM specimen, as presented in Figure 20. This value is far inferior to that of CFRP. Because of the stress concentration around the edge of butt splice, matrix crack propagation in CFRP occurred at a low strain level.

The gas leak rate of lap-splice CFRP/GM specimens without adhesive is presented in Figure 22. Gas leakage occurred at 1.0% for 5 mm of lap length specimen, and the gas leakage rate increased rapidly to $1.1 \times 10^{-7} \text{ Pa m}^3/\text{s}$. However, the onset of gas leak was about 1.1% for 2 mm lap length specimen; the leak rate did not increase rapidly. The gas leakage resistance of lap-splice specimens is better than that of the butt-splice

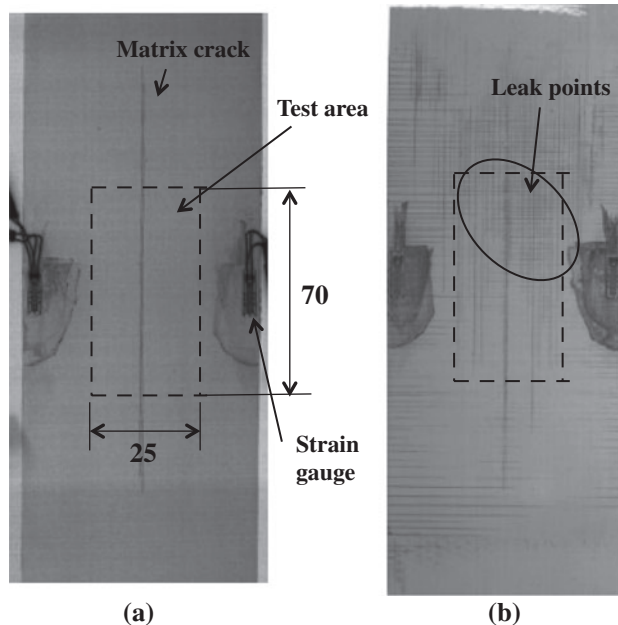


Figure 21. X-ray radiograms showing transverse cracks under uniaxial tensile loading. A longitudinal matrix crack was induced by the preliminary bending testing. (a) 0% tensile strain, (b) 0.9% tensile strain.

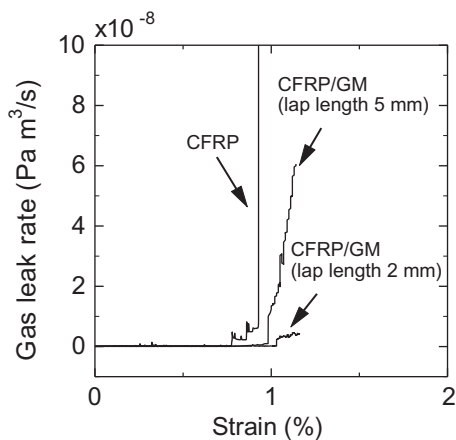


Figure 22. Helium gas leak behavior of lap slice Ti foil/CFRP without adhesive Lap length is 2 or 5 mm. No film adhesive was inserted to the lap splice joint.

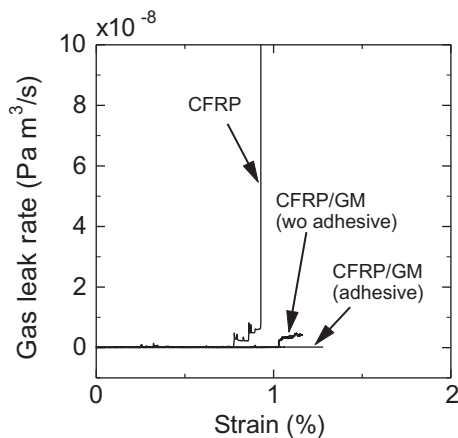


Figure 23. Helium gas leak behavior of adhesive lap splice joint of Ti-foil. Epoxy film adhesive (3M AF163) was inserted. The lap length was 2 mm.

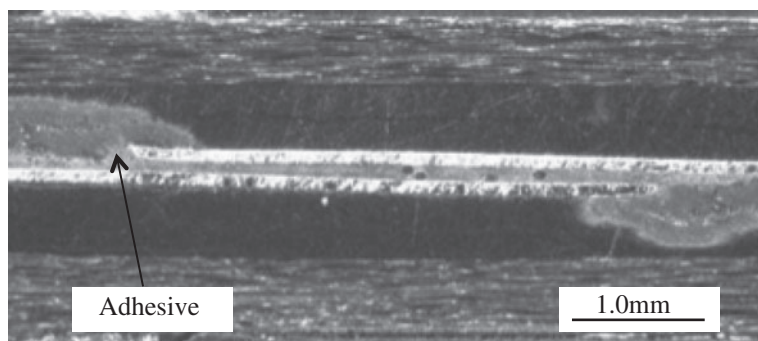


Figure 24. Optical micrograph showing microscopic voids around the adhesive lap splice joint of Ti-foil. The lap length is 2 mm. Adhesive flow from the lap splice is visible.

specimen. In the shorter lap splice (2 mm), epoxy resin flowing from prepreg contributes to the bonding of titanium foils, causing a lower gas leak rate.

Gas leakage of the lap-splice CFRP/GM with adhesive is presented in Figure 23. Titanium foil was bonded at the lap length (2 mm) using epoxy film adhesive. Gas leakage was not observed up to 1.25%, which is the failure strain. An optical micrograph showing the lap splice CFRP/GM specimen is presented in Figure 24. A few small voids are apparent. Adhesive flowing from the lap splice is visible. Gas leak resistance can be improved by controlling the quality of lap-splice bonding.

Titanium foil acts as a gas-tight layer. This suggests that a small amount of oxygen gas reaches titanium alloy through matrix cracks for a liquid oxygen tank application. However, the liquid oxygen never comes into contact with the Ti alloy directly. This situation is much better than COPV with a Ti alloy liner. CFRP/Ti composite has potential as cryogenic tank for liquid oxygen in addition to liquid hydrogen, LNG, and other propellants.

4. Conclusions

This study examined the processing and mechanical properties of titanium alloy foil-inserted cross-ply carbon fiber epoxy composites. Microscopic damage progression and helium gas leak behaviors were also investigated. The following conclusions were made:

- (1) Thermomechanical properties of cold-forged GM foils (Ti–36Nb–2Ta–3Zr–0.3O) were evaluated. GM foil exhibits considerable nonlinear pseudo-elastic behavior. The Young's modulus and CTE are, respectively, 70–80 GPa and $5.4\text{--}6.2 \times 10^{-6} \text{ K}^{-1}$. Extremely low elastic modulus and CTE, which are reported for cold-forged rod specimens, were not observed.
- (2) Titanium foil ($t=0.05$ or 0.1 mm) was embedded in cross-ply CFRP using co-curing process without adhesive. CFRP and titanium foil were well bonded by the epoxy resin in the prepreg. The strength and stress–strain behaviors under tensile and compressive loads were not affected to any considerable degree by GM foil insert in cross-ply CFRP.
- (3) Nonlinear stress–strain behavior of CFRP/GM is caused mainly by the nonlinear pseudo-elastic behavior of CFRP and GM. The stress–strain behavior and Young's modulus can be estimated using high-order stiffness and CLT up to the final failure.
- (4) Helium gas leakage of cross-ply CFRP occurred around 0.8% of tensile strain, although no gas leakage was observed up to 1.4% for CFRP/GM. However, gas leakage at 0.4% strain was observed for the butt-splice specimen. Results suggest that lap-splicing of titanium foil is effective to improve the gas leak resistance.

References

- [1] Torano Y, Arita M, Takahashi H, Arima K, Namiki F, Taniguchi T. Current study status of the advanced technologies for the J-I upgrade launch vehicle – cryogenic composite tank. AIAA paper 2001–1877; 2001.

- [2] Arritt BJ, Wegner PM, Fosness ER, Guerrero J, Buckley S. Composite tank development efforts at the Air Force Research Laboratory Space Vehicles Directorate. AIAA paper 2001–4606; 2001.
- [3] Messinger R, Pulley J. Thermal–mechanical cyclic test of a composite cryogenic tank for reusable launch vehicles. AIAA paper 2003–1766; 2003.
- [4] Higuchi K, Takeuchi S, Sato E, Naruo Y, Inatani Y, Namiki F, Tanaka K, Watabe Y. Development and flight test of metal-lined CFRP cryogenic tank for reusable rocket. *Acta Astronaut.* 2005;57:432–437.
- [5] Morino Y, Shimoda T, Morimoto T, Ishikawa T, Aoki T. Applicability of CFRP materials to the cryogenic propellant tank for reusable launch vehicle (RLV). *Adv. Compos. Mater.* 2001;10:339–347.
- [6] Kumazawa H, Aoki T, Susuki I. Analysis and experiment of gas leakage through composite laminates for propellant tanks. *AIAA J.* 2003;41:2037–2044.
- [7] Yokozeki T, Aoki T, Ishikawa T. Experimental cryogenic gas leakage through damaged composite laminates for propellant tank application. *J. Spacecraft Rockets.* 2005;42:363–365.
- [8] Yokozeki T, Ogasawara T. Evaluation of gas leakage through composite laminates with multilayer matrix cracks: cracking angle effects. *Compos. Sci. Technol.* 2006;66:2815–2824.
- [9] Bechel V, Negilski M, James J. Limiting the permeability of composites for cryogenic application. *Compos. Sci. Technol.* 2006;66:2284–2295.
- [10] Roy S, Benjamin M. Modeling of permeation and damage in graphite/epoxy laminates for cryogenic fuel storage. *Compos. Sci. Technol.* 2004;64:2051–2065.
- [11] Takeuchi S, Sato E, Onoda J, Higuchi K, Arakawa Y. Evaluation of adhesive bonding structure in cryogenic composite tank based on fracture mechanics. *Trans. Jpn. Soc. Aero. Space Sci.* 2009;52:36–46.
- [12] Suemasu H, Maeda Y, Namiki F, Inagi S. On initiation and growth of debonding between liner and FW layer of cryogenic composite material tank for rocket system due to nonuniform liner thickness. *J. Jpn. Soc. Compos. Mater.* 2006;32:237–243, in Japanese.
- [13] Wu G, Yang J-M. The mechanical behavior of GLARE laminates for aircraft structures. *J. Miner.* 2005;57:72–79.
- [14] Dennis A, Mark S. Delamination growth from face sheet seams in cross-ply titanium/graphite hybrid laminates. *Compos. Sci. Technol.* 2001;61:261–269.
- [15] Kolesnikov B, Herbeck L, Fink A. CFRP/titanium hybrid material for improving composite bolted joints. *Compos. Struct.* 2007;83:368–380.
- [16] Nakatani H, Kosaka T, Osaka K, Sawada Y. Damage characterization of titanium/GFRP hybrid laminates subjected to low-velocity impact. *Composites Part A.* 2011;42:772–781.
- [17] Grimsley BW, Cano RJ, Johnston NJ. Hybrid composites for LH2 fuel tank structure. Proceedings of 33rd ISTC (International SAMPE Technical Conference); Seattle, WA; 2001.
- [18] Arai N, Ogasawara T, Yokozeki T, Ogawa T. Mechanical properties of CFRP/Ti-alloy laminated composites. Proceedings of the 16th International Conference on Composite Materials (ICCM-16); Kyoto, Japan; 2007, CD-ROM.
- [19] Nishino K. Super multifunctional alloy “Gum Metal”. *R&D Rev. Toyota CRDL.* 2003;38:50.
- [20] Saito T, Furuta T, Hwang J-H, Kuramoto S, Nishino K, Suzuki N, Chen R, Yamada A, Ito K, Seno Y, Nonaka T, Ikehata H, Nagasako N, Iwamoto C, Ikuhara Y, Sakuma T. Multifunction alloys obtained via a dislocation-free plastic deformation mechanism. *Science.* 2003;300:464–467.
- [21] Ogasawara T, Ishida Y, Yokota R, Watanabe T, Aoi T, Goto J. Processing and properties of carbon fiber/Triple-A polyimide composites fabricated from imide oligomer dry prepreg. *Composites Part A.* 2007;38:1296–1303.
- [22] Ishikawa T, Matsushima M, Hayashi Y. Hardening non-linear behaviour in longitudinal tension of unidirectional carbon composites. *J. Mater. Sci.* 1985;20:4075–4083.
- [23] Hill R. The mathematical theory of plasticity. London: Oxford University Press; 1950.
- [24] Chen J-L, Sun C-T. A plastic potential function suitable for anisotropic fiber composites. *J. Compos. Mater.* 1993;27:1379–1390.
- [25] Kuramoto S, Furuta T, Hwang J, Nishino K, Saito T. Elastic properties of Gum Metal. *Mater. Sci. Eng. A.* 2006;442:454–457.

- [26] Tallinga RJ, Dashwoodb RJ, Jacksonc M, Dyea D. On the mechanism of superelasticity in Gum Metal. *Acta Mater.* 2009;57:1188–1198.
- [27] Yokozeki T, Ogasawara T, Ishikawa T. Nonlinear behavior and compressive strength of unidirectional and multidirectional carbon fiber composite laminate. *Composites Part A.* 2006;37:2069–2079.
- [28] Whitney JM. Effective elastic constants of bidirectional laminates containing transverse ply cracks. *J. Compos. Mater.* 2003;34:954–978.
- [29] Curtis GJ, Milne JM, Reynolds WN. Non-Hookean behavior of strong carbon fibers. *Nature.* 1968;220:1024–1025.